Materials Today Physics 35 (2023) 101129

Contents lists available at ScienceDirect

Materials Today Physics

journal homepage: www.journals.elsevier.com/materials-today-physics

Study of the defect chemistry in Ag_2Q (Q = S, Se, Te) by first-principles calculations

Hexige Wuliji [a], Kunpeng Zhao [a,**], Xiaomeng Cai [b], Huirong Jing [b], Yaowei Wang [b], Haoran Huang [a], Tian-Ran Wei [a], Hong Zhu [b,***], Xun Shi [a,c,*]

[a] State Key Laboratory of Metal Matrix Composites, School of Materials Science and Engineering, Shanghai Jiao Tong University, Shanghai, 200240, China
[b] University of Michigan-Shanghai Jiao Tong University Joint Institute, Shanghai Jiao Tong University, Shanghai, 200240, China
[c] State Key Laboratory of High Performance Ceramics and Superfine Microstructure, Shanghai Institute of Ceramics, Chinese Academy of Sciences, Shanghai, 200050, China

A R T I C L E I N F O

Keywords:
Thermoelectric
Silver chalcogenides
Defect chemistry
Doping
Interstitial

A B S T R A C T

Ag_2Q-based (Q = S, Se, Te) silver chalcogenides show great potential in thermoelectrics due to their suitable band gaps, high electron mobilities, and even remarkable ductility. Particularly, Ag_2S and Ag_2S/Se/Te solid solutions have been reported with both good ductility and thermoelectric performance, which are extremely suitable for the application in flexible wearables. However, the underlying mechanism of the native n-type conduction and p-type undopability for Ag_2Q remains elusive. Herein, we use first-principles calculations based on density functional theory combined with *GW* correction to investigate the defect chemistry in Ag_2Q. It is found that the site potential and Voronoi volume deviations resulting from Ag interstitials are noticeably smaller than those caused by Ag vacancies, which makes Ag interstitials with low formation energy more desirable during preparation, contributing to the native n-type conduction. The small and even negative dopability windows, on the other hand, account for the p-type undopability of Ag_2Q. The calculated carrier concentrations of pristine Ag_2Q are well consistent with the experimental observations, validating the reliability of our defect calculations. This work provides valuable guidance for first-principles calculation of defect chemistry in other narrow-gap semiconductors.

1. Introduction

Semiconductors, which have unique electrical properties between that of a conductor and an insulator, are the brains of modern electronics. One of the remarkable characteristics of a semiconductor is that its conducting behaviors can be altered by intrinsic (e.g., interstitials or vacancies) or extrinsic doping (e.g., foreign elements) in the crystal lattices. It is called n-type when the doped semiconductor contains free electrons, and it is known as p-type when it contains free holes. Both n-type and p-type semiconductors are needed for electronic applications like thermoelectrics, photovoltaics, and transistors [1–3] [1–3] [1–3]. However, experimentally, it is found that some semiconductors can only be doped with either n-type or p-type. For instance, nearly all Ag-based chalcogenides exhibit solely n-type conduction behavior, while most Cu-based chalcogenides demonstrate only p-type conduction [4,5]. It is essential to reveal the defect chemistry and conduction type of semiconductors to realize their full potential and to guide the experimental design.

Binary Ag_2Q (Q = S, Se, Te) semiconductors, a promising thermoelectric (TE) material family, have attracted widespread interest in virtue of their complex crystal structures, suitable band gaps, and high electron mobilities [6,7]. High TE figure of merit zT values up to 1.2 and 1.4 have been achieved near room temperature in Ag_2Se and Ag_2Te, respectively [8,9]. The inorganic Ag_2S was found to exhibit unexpectedly good malleability at room temperature, showing great potential in flexible/wearable electronics [10,11]. The TE performance of pristine Ag_2S is not satisfactory due to its low electrical conductivity. However, by alloying with certain amount of Se or Te, the zT value of Ag_2S could

* Corresponding author. State Key Laboratory of Metal Matrix Composites, School of Materials Science and Engineering, Shanghai Jiao Tong University, Shanghai, 200240, China.
** Corresponding author.
*** Corresponding author.
E-mail addresses: zkp.1989@sjtu.edu.cn (K. Zhao), hong.zhu@sjtu.edu.cn (H. Zhu), xshi@mail.sic.ac.cn (X. Shi).

https://doi.org/10.1016/j.mtphys.2023.101129
Received 8 April 2023; Received in revised form 16 May 2023; Accepted 25 May 2023
Available online 26 May 2023

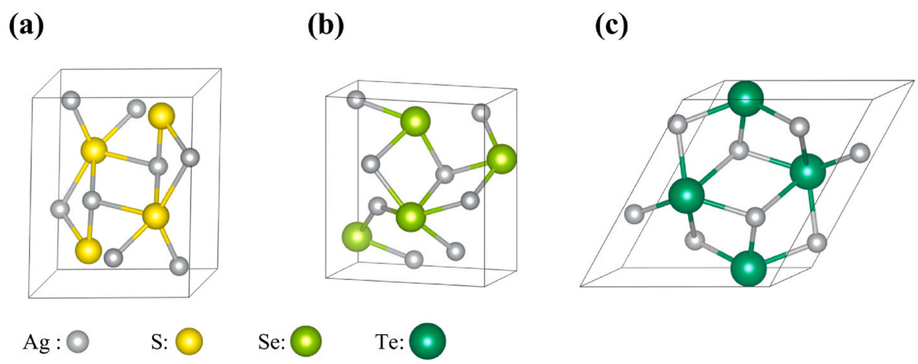

Fig. 1. Crystal structures of low-temperature Ag_2Q: (a) Ag_2S, (b) Ag_2Se, (c) Ag_2Te.

be also improved to 0.4 at 300 K, while maintain material's excellent ductility or plasticity [12–15] [12–15] [12–15]. Theoretically, the stoichiometric Ag_2Q should be intrinsic semiconductors, whereas the experimentally obtained Ag_2Q samples are generally self-doped and exhibit n-type conduction behaviors. The origin of native n-type conduction, i.e. the intrinsic defects, have not been unambiguously determined from the experimental or theoretical perspective. On the other hand, although the electron concentrations of Ag_2Q could be tuned by approaches like non-stoichiometric synthesis [16,17] or elemental doping [18,19], its conduction type could not be reversed. The reasons of the permanent n-type behavior and p-type undopability for Ag_2Q are still unclear.

Although a few theoretical efforts (defect calculations) have been made to reveal the defect chemistry and dopability in Ag_2S, the obtained results are inconsistent and even contradictory. For instance, a mono-vacancy calculation showed that the zero-charged vacancy formation energy of Ag is about two times lower than that of S in monoclinic Ag_2S [20], while another DFT calculation showed that the donor-like charged S vacancies have lower formation energies [21]. As for Ag_2Se and Ag_2Te, there are still no studies on their defect calculations. The main reason is that Ag_2Se and Ag_2Te have rather low band gaps (about 0.1 eV [22,23]), which pose a big challenge to calculate defect properties accurately by

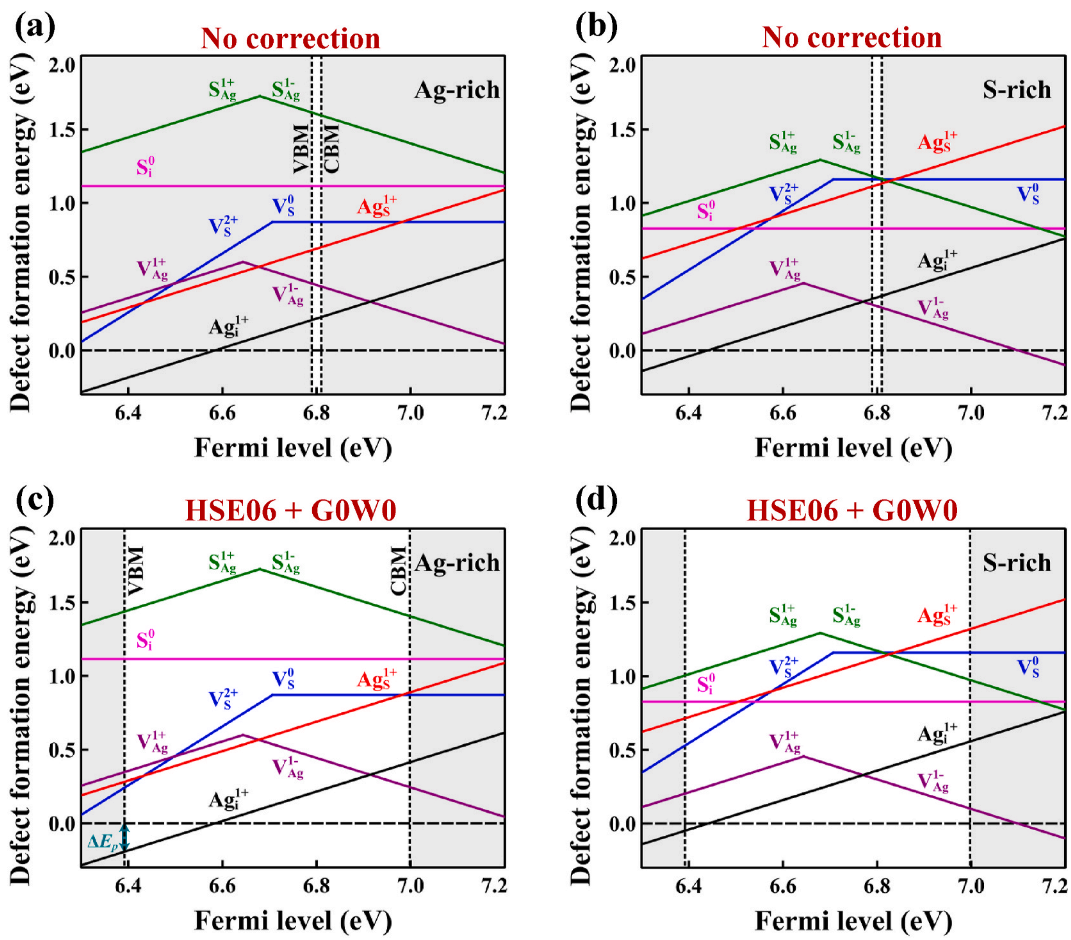

Fig. 2. Formation energies of native defects as functions of Fermi energy for Ag_2S. Formation energies calculated using the PBE + U + vdW without corrections at (a) Ag-rich and (b) S-rich conditions. Formation energies calculated using HSE06 + G0W0 corrections at (c) Ag-rich and (d) S-rich conditions. The line slope is equal to the defect charge state. The positions of VBM and CBM are denoted by the vertical dotted lines in each figure. The p-type dopability window (ΔE_p) is defined at the VBM in Fig. 2c.

using standard DFT methods due to the underestimation of band gaps caused by standard local density (LDA) or generalized gradient approximation (GGA). Hybrid functionals enable more accurate prediction of the band gap for semiconductors and insulators [24], but are challenging to accurately predict the band-edge positions for narrow-gap systems [25]. The more accurate GW calculation is rather time-consuming, especially for the defect calculations of large supercell with dilute doping limits [26,27]. Recently, a robust band-alignment strategy was proposed, which utilized GW calculations to resolve band-gap issues and incorporated a correction method for finite-size effects in the supercell approach [28]. It has been proven that the standard LDA and GGA can yield similar results in terms of defect properties compared to hybrid functionals, provided that equivalent GW band-edge corrections are applied [29]. By utilizing these ex post facto corrections for supercell defect calculations, recent advances have been made in accurately calculating defects in narrow-gap TE materials with gap values less than 1.0 eV, such as $KGaSb_4$ [30], PbTe [31], and BiCuSeO [32].

In this work, we perform first-principles calculations based on standard DFT methods combined with GW band-edge correction to comprehensively investigate the defect chemistry and dopability of Ag_2Q. It is found that the most favorable Ag interstitials, among all intrinsic defects, are responsible for the native n-type conduction of Ag_2Q. The small and even negative p-type dopability window suggest difficulty in p-type doping. The analysis of site potential, Voronoi volume, and charge density confirms that Ag interstitials are more likely to be produced during the synthesis process than Ag vacancies.

2. Computational methods

All DFT calculations of low-temperature Ag_2Q were performed by utilizing the Vienna *Ab initio* Simulation Package (VASP) code [33]. The interaction between ion cores and valence electrons were treated with the projector augmented wave (PAW) method [34]. To accurately reproduce the lattice parameters that closely match experimental data, various exchange-correlation functionals were applied, such as the Perdew Burke Ernzerhof (PBE) within GGA [35], SCAN [36], and the hybrid functionals proposed by Heyd, Scuseria, and Ernzerhof (HSE06) [37]. For the layered structure of Ag_2S, van der Waals (vdW) forces were included by adding the DFT-D3 correction with Becke-Johnson damping function [38] in PBE and rVV10 [39] in SCAN to consider the non-local electron correlation. The plane wave energy cutoff was set to 520 eV for all calculations except for the default value used for HSE06. A rotationally invariant approach to implement the Hubbard U [40] was adopted to describe the on-site Coulomb interactions in Ag 4*d* orbitals.

2.1. The identification of hubbard U

To identify the Hubbard U parameters for the Ag 4*d* orbitals in the low-temperature Ag_2Q systems, we carried out the linear response calculations based on the constrained LDA (cLDA) method [41] for the low-temperature Ag_2Q, metallic Ag and cubic Ag_2O. According to our calculations and previous studies [42,43], we chose $U = 3$ eV for Ag 4*d* orbitals. Moreover, by comparing the lattice parameters of orthorhombic Ag_2Se obtained from different U via SCAN + U method with experimental data, it is found that the proper U value is in good agreement with our cLDA calculations, and the results are shown in Table S1 and Fig. S1 ~ 4.

2.2. Structure relaxation

Each Ag_2Q compound undergoes a phase transition near room temperature from the low-symmetry ordered structure to the high-symmetry disordered structure [44,45]. At low temperatures, both Ag_2S and Ag_2Te crystallize in monoclinic structures with space group of $P2_1/c$, while Ag_2Se crystallizes in an orthorhombic structure with space group of $P2_12_12_1$. At high temperatures, all of them transform into cubic structures with Ag ions disorderedly distributed among the rigid anionic sublattice [46]. In this work, all the calculations were performed on the low temperature ordered structure of Ag_2Q. The low-temperature crystal structures of Ag_2Q obtained from experimental references [47–49] [47–49] [47–49] (as shown in Fig. 1) were fully relaxed until the energy convergence criterion reached 10^{-6} eV. The relaxed lattice parameters compared with the experimental data are shown in Table S2 ~ S4. For Ag_2Se and Ag_2Te, it is found that the PBE + U method without vdW correction can produce lattice parameters that are as precise as those obtained using the SCAN + U method, which are in good agreement with experimental data (with errors <2%). However, it is necessary to add vdW correction for Ag_2S due to its layered structure. To ensure computational consistency across all three Ag_2Q compounds, we selected the PBE + U method with D3 vdW correction for Ag_2S. The obtained results, alike those obtained using SCAN + U with rVV10 correction, slightly deviate from the experimental data (with errors ~ 3%).

2.3. Defect formation energy calculation

The formation energies of intrinsic point defects in Ag_2Q such as Ag and Q anion vacancies, interstitials, antisites were calculated by using the standard supercell approach [50]. The Python Charged Defect Toolkit (PyCDT) [51] was utilized to construct all the defective supercell structures based on the relaxed primitive cells of Ag_2Q. The total energies of the host and all defect structures were calculated in 3 × 2 × 2 supercells with 144 atoms by using PBE + U method (for Ag_2S, vdW correction were added). For each defect considered, all possible configurations within Ag_2Q supercells were constructed by PyCDT and the most stable defective structures with zero charge state were selected for further structural relaxations by comparing total energies. A 2 × 2 × 2 Γ-centered k mesh based on the convergence tests (shown in Fig. S5) and a residual atomic force convergence criterion of 10^{-2} eV/Å were employed to relax the atomic positions within a fixed cell shape and volume for all defect structures. The formation energy for a charged point defect can be calculated using

$$E_{\mathrm{form}} = E_{\mathrm{tot}}(d,q) - E_{\mathrm{tot,host}} + \sum_i n_i\mu_i + q(\varepsilon_{\mathrm{F}} + E_{\mathrm{V}}) + E_{\mathrm{corr}} \quad (1)$$

where $E_{\mathrm{tot}}(d,q)$, $E_{\mathrm{tot,host}}$, n_i, μ_i, ε_{F}, E_{V} and E_{corr} are the total energy of the structure with defect d in charge state q, the total energy of the host Ag_2Q, the change in the number of atoms i added ($n_i < 0$) or removed ($n_i > 0$), the chemical potential of element i, the Fermi energy level referred to the valence band maximum (VBM), the VBM value, and finite-size corrections, respectively. Based on the formula $\mu_i = \mu_i^0 + \Delta\mu_i$, the chemical potential μ_i is determined by the reference value of the constituent i in the standard phase (μ_i^0) and the deviation ($\Delta\mu_i$). Under equilibrium growth conditions, chemical potentials must maintain the stable Ag_2Q by avoiding precipitation of the pure elemental substances and other competitive compounds if extrinsic dopants are introduced [32]. Therefore, the chemical potentials should satisfy the limitation $2\Delta\mu_{\mathrm{Ag}} + \Delta\mu_{\mathrm{X}} = \Delta H_{\mathrm{form}}(\mathrm{Ag_2Q})$, where $\Delta\mu_{\mathrm{Ag}} \leq 0$ and $\Delta\mu_{\mathrm{Q}} \leq 0$. The finite-size corrections were applied following the methodology by Freysoldt [52], which included image-charge corrections for charged defects and potential alignment corrections. GW calculations including single shot quasiparticle G0W0, partially self-consistent GW0 and those combined with HSE06 based on PBE + U (for Ag_2S, vdW effects were considered) were applied to correct the band edge levels and band gaps for the primitive cells of low-temperature Ag_2Q. It should be noted that GW corrections can potentially impact the total energies. However, the impact of GW corrections on the defect formation energy, which refers to the energy difference between bulk and defected structures while considering chemical potentials, may be negligible. Moreover, the single shot quasiparticle G0W0 and partially self-consistent GW0 cannot

Table 1
The VBM positions (eV) and band gaps (E_g, eV) of Ag_2Q calculated by different methods. "No correction" represents PBE + U + vdW for Ag_2S and PBE + U for Ag_2Se and Ag_2Te. All the correction methods (G0W0, GW0, HSE06+G0W0, and HSE06+GW0) are applied based on the standard PBE + U (+vdW) methods. The electrostatic potentials of Ag_2Q calculated via different methods are aligned at the same levels. The experimental data are also included for comparison [10,22,23,56].

Methods	Ag_2S		Ag_2Se		Ag_2Te	
	E_g	VBM	E_g	VBM	E_g	VBM
No correction	0.0202	6.7899	0.0189	5.3337	−0.0023	6.3430
G0W0	0.2504	6.6431	0.0461	5.1924	0.0106	6.2182
GW0	0.2822	6.6270	**0.0587**	**5.1634**	**0.0709**	**6.1734**
HSE06+G0W0	**0.6057**	**6.4072**	0.0271	5.0071	−0.1104	5.9819
HSE06+GW0	0.5697	6.5151	0.0307	5.0951	−0.2592	6.0848
Exp [10,22,23,56].	0.8–1.0	–	0.07–0.18	–	0.02–0.07	–

provide total energy calculations at present [25].

In HSE06 based on PBE, the exchange part (E_x) consists of a linear combination of Hartree-Fock (HF) and semilocal PBE while the correlation part (E_{xc}) remains PBE, which is described as

$$E_{xc}^{hybrid} = \alpha E_x^{HF} + (1-\alpha)\alpha E_x^{PBE} + E_c^{PBE}$$

where α represents the mixing parameter that determines the relative amount of HF and PBE. To investigate the effect of mixing parameter on band gaps of Ag_2Q systems, the mixing parameter was chosen as 0.25 (by default), 0.3, 0.4, 0.45, and 0.5 in this work.

2.4. Electrostatic site potentials, voronoi volumes, and band unfolding calculations

To illustrate the effects on the lattice distortion caused by Ag interstitials and vacancies in orthorhombic Ag_2Se as a case study of Ag_2Q family, the differences of electrostatic site potentials from the wave function derived Mulliken charges and Voronoi volumes of atoms in 3 × 2 × 2 supercell between the host and defect structures were calculated by using LOBSTER [53] and the Python materials Genomics (Pymatgen) [54] codes, respectively. In addition, the unfolded band structures of the host and defect structures including one Ag interstitial or one Ag vacancy in Ag_2Se 3 × 2 × 2 supercells were calculated by using the modified Becke-Johnson method and futherly analyzed by the VASPKIT [55] code.

3. Results and discussion

3.1. Band-edge corrections for Ag_2Q

Correcting the band-edge positions and band gaps is crucial for accurate defect calculations, because a small deviation in these parameters may lead to qualitatively different conclusions concerning the conduction type and dopability. The calculated VBM positions and band-gap values of Ag_2Q via the standard PBE + U method (for Ag_2S, the vdW effects are added) without any corrections (denoted as "No correction") and with G0W0, GW0, HSE06 + G0W0, and HSE06 + GW0 corrections are listed in Table 1.

The calculated band gap of Ag_2S via the standard PBE + U + vdW method is only 0.0202 eV, which is much lower than the experimental value of ~0.9 eV [10]. After correcting the band-edge positions using single-shot G0W0 or partially self-consistent GW0 methods, the resulting band gaps are improved to 0.2504 and 0.2822 eV, respectively. However, even with these corrections, the band gap remains too small when compared to experimental data. Nonetheless, other methods such as HSE06 + G0W0 and HSE06 + GW0 based on PBE + U + vdW yield band-gap values of 0.6057 and 0.5697 eV, respectively, which are closer to the experimental gap value. Among these methods, HSE06 + G0W0 can lower the valence band maximum (VBM) by 0.3827 eV and raise the conduction band minimum (CBM) by 0.223 eV compared to PBE + U, leading to a band gap of 0.6057 eV, which is much closer to experimental data than HSE06 + GW0. Therefore, we chose HSE06 + G0W0 as the method for correcting the band edge and band gap of Ag_2S in this study. The same method was also used in a previous work for PbTe [31], which has a band-gap value similar to Ag_2S.

According to previous studies, the experimental band gap of Ag_2Se is very small, ranging from 0.07 to 0.18 eV [22,56]. In this work, we employed various correction methods, including G0W0, GW0, HSE06 + G0W0, and HSE06 + GW0, to calculate the band-edge positions and band gaps for Ag_2Se. The obtained E_g values are listed in Table 1. As can be seen that both HSE06 + G0W0 and HSE06 + GW0 are less accurate than pure G0W0 and GW0 for Ag_2Se, which is in contrast to the results for Ag_2S. While all the calculated results are smaller than the experimental E_g, the partially self-consistent GW0 calculation based on the PBE + U method, with a band-gap value of 0.0587 eV, is closest to the reported value [22]. Therefore, we selected GW0 as the correction method for band-edge alignment in our study of Ag_2Se.

For monoclinic Ag_2Te, the experimental band-gap value is about 0.02–0.07 eV [23], which is even smaller than that of orthorhombic Ag_2Se. The calculated band-gap values of Ag_2Te using different methods are more complicated. The E_g obtained from PBE + U for Ag_2Te is negative (−0.0023 eV), an indicative of semi-metallic character [44,57]. Correcting the band gap using HSE06 + G0W0 or HSE06 + GW0 leads to an even more negative E_g, while positive E_g values of 0.0106 and 0.0709 eV are achieved when using G0W0 and GW0 calculations based on PBE + U method, which are sufficiently proper when considering only the band-gap value. However, the downward shift of both the VBM and CBM to lower energy levels has a large impact on the conductive behavior of Ag_2Te, as will be discussed in the next section.

To investigate the effect of mixing parameter on band-edge levels and band gaps of Ag_2Q, HSE06 calculations with different mixing parameters were applied. It was found that the choice of mixing parameters indeed has a large effect on the band gap values, which gradually increase with increasing mixing parameter α (see Table S5). However, the band-edge position of VBM is too low compared with those calculated from pure PBE + U, leading to over-corrections for defect formation energies in Ag_2Q systems. Previous study showed similar results that solely changing the mixing parameters could make some errors for band edge levels [25].

3.2. Intrinsic defect formation energies of Ag_2Q

The formation energies of intrinsic defects with favorable charge states q for Ag_2Q are calculated by using PBE + U (for Ag_2S, PBE + U + vdW) method with and without GW band-edge corrections. Various possible defects, including Ag and anion (Q) interstitials (Ag_i^q, Q_i^q), vacancies (V_{Ag}^q, V_Q^q), and antisites (Ag_Q^q, Q_{Ag}^q, the subscript represents the original lattice sites to be replaced), are taken into consideration.

Our calculation results show that the donor Ag_i^{1+} and acceptor V_{Ag}^{1-} are the predominant native defects for Ag_2S. When using the PBE + U + vdW method, the Fermi level is pinned by Ag_i^{1+} and V_{Ag}^{1-} in the conduction band at Ag-rich condition, and in the valence band at S-rich condition (see Fig. 2a and b). It means Ag_2S exhibits n-type conduction at Ag-rich condition and p-type conduction at S-rich condition, which is

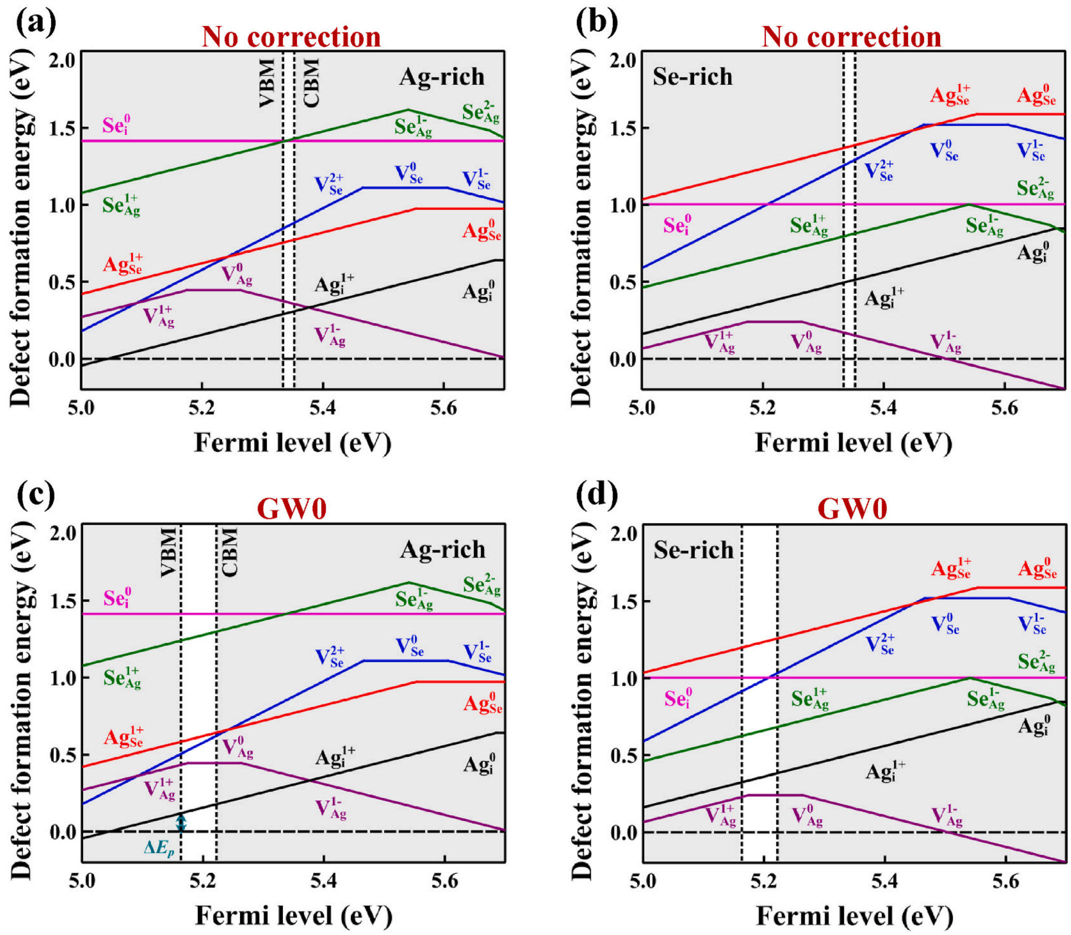

Fig. 3. Formation energies of native defects as functions of Fermi energy for Ag_2Se. Formation energies calculated using the PBE + *U* without corrections at (a) Ag-rich and (b) Se-rich conditions. Formation energies calculated using GW0 corrections at (c) Ag-rich and (d) Se-rich conditions. The line slope is equal to the defect charge state. The positions of VBM and CBM are denoted by the vertical dotted lines in each figure. The p-type dopability window (ΔE_p) is defined at the VBM in Fig. 3c.

incongruent with experimental observations. However, by applying HSE06 + G0W0 band-edge correction based on PBE + *U* + vdW, the formation energies of Ag interstitials and Ag vacancies cross in the band-gap region, which pins the Fermi level close to CBM at both Ag-rich and S-rich conditions (see Fig. 2c and d). Consequently, Ag_2S permanently exhibits n-type conduction, in accordance with experimental results. The p-type dopability of a material can be gauged from the energy window (ΔE_p, see Fig. 2c) at the valence band minimum determined by the lowest-energy native donor defect. The lower the dopability window, the more difficulty for p-type doping. The ΔE_p of Ag_2S calculated from HSE06 + G0W0 at both Ag-rich and S-rich condition are negative, indicating that p-type doping is infeasible for Ag_2S [32].

According to the formation energy calculated from the standard PBE + *U* method, the donor-like Ag interstitials are the dominant defects under Ag-rich condition, while acceptor-like Ag vacancies are the dominant defects under Se-rich conditions in Ag_2Se. The presence of donor-like Ag interstitials is responsible for the n-type conductive behavior in Ag_2Se, which agrees with experimental findings. However, the acceptor-like Ag vacancies at the Se-rich condition yield p-type conductive behavior, which is inconsistent with experiments. After correcting the band-edge using GW0, the charge state of Ag vacancies becomes zero in the whole band-gap region (see Fig. 3c), indicating Ag vacancies no longer exhibit acceptor-like characters. As a result, the system exhibits n-type conductive behavior under both Ag-rich and Se-rich conditions, which well explains the observed permanent n-type conduction in experiments. The presence of favorable Ag interstitials and vacancies suggests the possible existence of Frenkel defects in the Ag_2Se lattice. Moreover, the p-type dopability window for Ag_2Se, with or without band-edge corrections, is quite narrow that explains why Ag_2Se is p-type undopable.

Similar to Ag_2S and Ag_2Se, Ag interstitials and Ag vacancies are the most prevalent defects in monoclinic Ag_2Te. According to the PBE + *U* method results, Ag vacancies remain zero charge at VBM and thus contribute little to extra carriers (see Fig. 4a and b). Donor-like Ag interstitials, on the other hand, are the primary source of charge carriers. By utilizing GW0 band-edge correction based on PBE + *U* calculations, while the band-gap is open, both VBM and CBM shift down to lower energy levels, resulting in the positive charged Ag vacancies (see Fig. 4c and d). Consequently, Ag_2Te exhibit n-type conduction at both Ag-rich and Te-rich conditions, which is also consistent with the experimental observations. Nonetheless, it should be noted that the donor-like Ag vacancies in the band-gap region is somehow contrary to common chemical insights. Defect calculations on such narrow-dap or even closed-gap systems are extremely challenging, and more robust but time-consuming methods such as meta-GGA or hybrid functionals in combination with GW quasiparticle theory may be necessary to resolve this problem in the future.

3.3. *Effects of main intrinsic defects in Ag_2Se*

Based on the above calculations, it appears that the main defects in Ag_2Q are the Ag interstitials and vacancies, which have quite low formation energies. To gain more insight into the formation of these defects, we examine the effects of Ag interstitials and vacancies on the

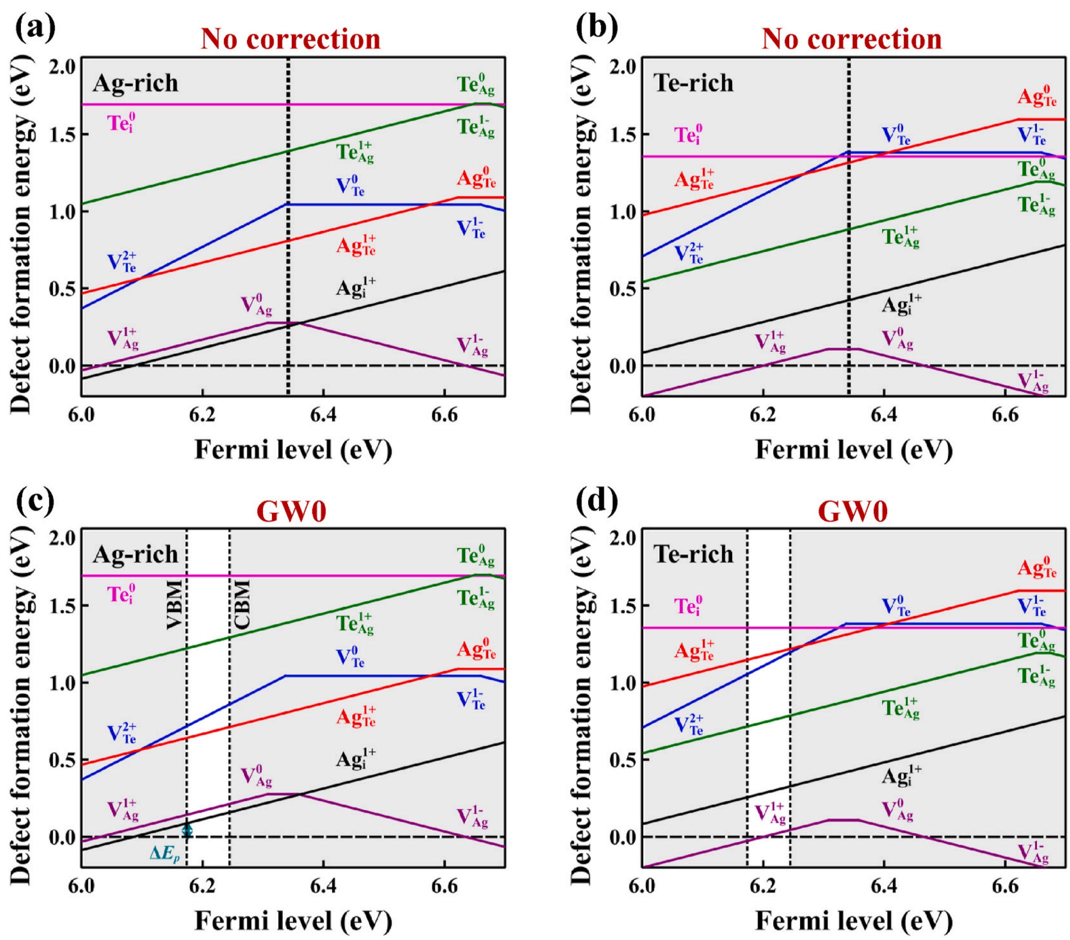

Fig. 4. Formation energies of native defects as functions of Fermi energy for Ag_2Te. Formation energies calculated using the standard PBE + U without corrections at (a) Ag-rich and (b) Te-rich conditions. Formation energies calculated using GW0 corrections at (c) Ag-rich and (d) Te-rich conditions. The line slope is equal to the defect charge state. The positions of VBM and CBM are denoted by the vertical dotted lines in each figure. The p-type dopability window (ΔE_p) is defined at the VBM in Fig. 4c.

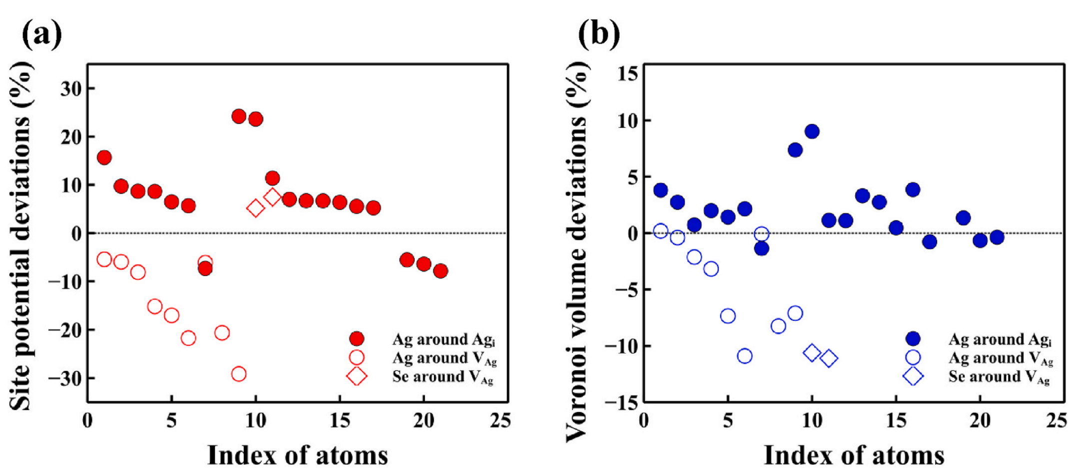

Fig. 5. (a) Atomic site potential deviations and (b) Voronoi volume deviations around the defects (Ag interstitials and vacancies) in Ag_2Se. The site potential deviations greater than 5% are taken as the threshold for lattice distortion.

lattice distortion, charge density, electronic structure by taking Ag_2Se as a case study.

Lattice distortions in defect structures can be assessed through the analysis of atomic site potential and Voronoi volume deviations around the defects. As shown in Fig. 5, the site potential and Voronoi volume deviations caused by the Ag interstitials are obviously smaller than those of Ag vacancies, suggesting a comparatively smaller degree of lattice distortion around Ag interstitials. Moreover, the Ag interstitials have little impact on the Se anions, which is dissimilar to Ag vacancies. The electron localization function (ELF) analysis shows that the interstitial Ag atoms form chemical bonds with Se atoms and adjacent Ag atoms, which can stabilize the defect structure. In contrast, Ag vacancies cause

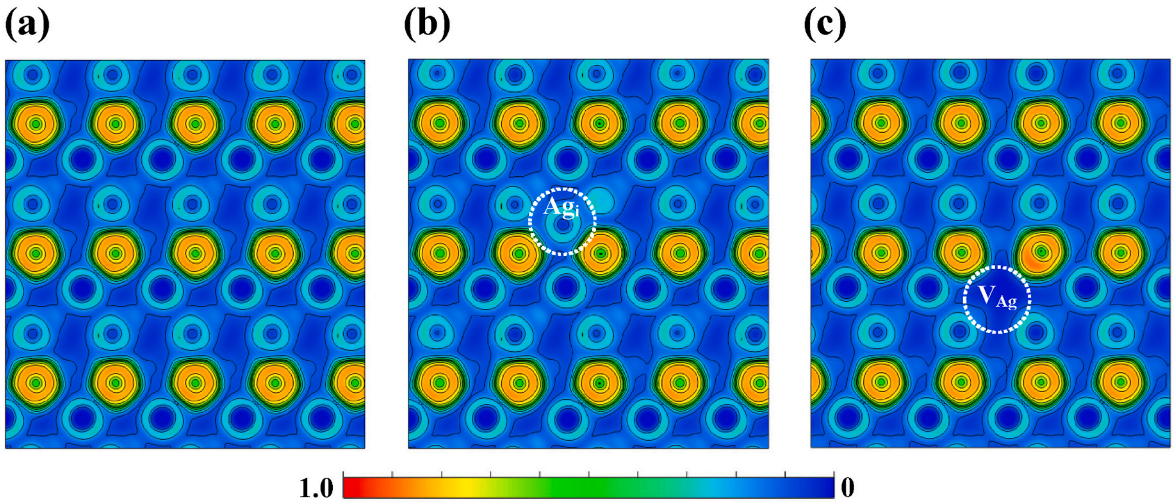

Fig. 6. ELF of the host and defective orthorhombic Ag_2Se: (a) host Ag_2Se with $3 \times 2 \times 2$ supercell, (b) Ag_2Se with one Ag interstitial and (c) one Ag vacancy in $3 \times 2 \times 2$ supercell.

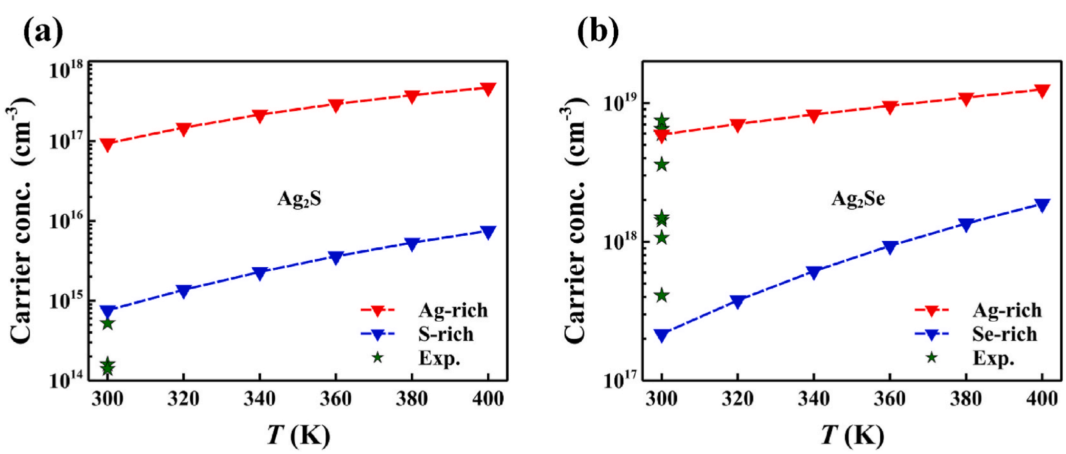

Fig. 7. Calculated carrier (electron) concentration as a function of temperature for self-doped (a) Ag_2S and (b) Ag_2Se at Ag-rich and Q-rich conditions. The experimental results are included for comparison [10,12,17,56,59] [10,12,17,56,59–63] [10,12,17,56,59–63].

lattice distortion of surrounding atoms in ELF (see Fig. 6c), ultimately making the defect structure unstable. Based on the lattice distortions and ELF analysis, we can qualitatively conjecture that Ag interstitials are more likely to form in Ag_2Se than Ag vacancies. In addition, the band structure calculations (shown in Fig. S6) indicate that Ag interstitials can shift Fermi level toward the conduction band, which is responsible for n-type conductive behaviors for Ag_2Se, being consistent with the results of defect calculations.

3.4. Carrier concentrations of Ag_2S and Ag_2Se

Based on the intrinsic defect formation energies, we calculate the self-consistent Fermi level as well as carrier concentrations for Ag_2S and Ag_2Se. The over-correction of band-edge and ensuing donor-like Ag vacancies in Ag_2Te still remains problematic, and its carrier concentration is thus not calculated. The defect concentrations at given temperatures were calculated self-consistently by establishing charge neutrality [32], which is expressed as

$$\sum_{d^q}\left[qN_d e^{-\Delta E_{\mathrm{form}}/k_B T}\right] + p - n = 0 \quad (2)$$

where the sum runs over all defects d^q, N_d is the site concentrations where defects can be formed, k_B is the Boltzmann constant, T is the temperature, and p and n are the hole and electron concentrations, respectively. p and n are expressed as

$$p = \int_{-\infty}^{\mathrm{VBM}} \mathrm{g}(E)[1 - \mathrm{f}(E)]dE \quad (3)$$

$$n = \int_{\mathrm{CBM}}^{\infty} \mathrm{g}(E)\mathrm{f}(E)dE \quad (4)$$

where $\mathrm{f}(E)$ is the Fermi-Dirac distribution, and $\mathrm{g}(E)$ is density of states (DOS) of Ag_2Q calculated by using standard PBE + U method with rigid shifts of band edges according to the GW corrections in this work. The charge neutrality equations were solved by utilizing a numerical algorithm with calculating self-consistent Fermi level at given temperatures and modified DOS [58]. As shown in Fig. 7, the calculated electron concentrations at room temperature range from 7.6×10^{14} cm^{-3} (S-rich) to 9.4×10^{16} cm^{-3} (Ag-rich) for Ag_2S, which is slightly higher than the experimental data [10,12,59]. Such deviation may be caused by the underestimate of band-gap (see Table 1). It is possible to tune the band-gap value by changing the mixing parameters in hybrid functionals combing GW calculations if the enormous computational cost is acceptable. The calculated electron concentrations for Ag_2Se is 2.2×10^{17} cm^{-3} at Se-rich condition and 5.9×10^{18} cm^{-3} at Ag-rich condition (Fig. 7b), which are in fair agreement with experiments [17,56,60–63].

These results indicate our intrinsic defect calculations are qualitatively reliable.

4. Conclusions

In summary, we investigate the defect chemistry and dopability of Ag_2Q by performing first-principles defect calculations based on standard PBE + *U* methods combined with GW band-edge corrections. Our defect calculations reveal that the native n-type conduction and p-type undopability in Ag_2Q-based semiconductors are caused by the donor-like Ag interstitials with low formation energy and small dopability window. The calculated carrier concentrations are in accordance with the experimental findings. Although there still exist challenges in accurately calculating defect chemistry in narrow-gap semiconductors, this work qualitatively reveals the underlying mechanism of n-type conduction and p-type undopability for Ag_2Q.

Credit author statement

Hexige Wuliji: Methodology, Validation, Formal analysis, Investigation, Data curation, Writing – original draft, Visualization. Kunpeng Zhao: Conceptualization, Methodology, Supervision, Writing – review & editing, Project administration, Funding acquisition. Xiaomeng Cai: Methodology. Huirong Jing: Methodology. Yaowei Wang: Methodology. Haoran Huang: Methodology, Formal analysis. Tian-Ran Wei: Resources, Formal analysis. Hong Zhu: Conceptualization, Methodology, Formal analysis, Writing – review & editing. Xun Shi: Conceptualization, Writing – review & editing, Supervision, Funding acquisition.

Declaration of competing interest

The authors declare that they have no known competing financial interests or personal relationships that could have appeared to influence the work reported in this paper.

Data availability

Data will be made available on request.

Acknowledgments

This work was supported by the National Key Research and Development Program of China (No. 2017YFA0700705), National Natural Science Foundation of China (No. 52232010, 91963208 and T2122013), the Shanghai Pilot Program for Basic Research-Chinese Academy of Science, Shanghai Branch (JCYJ-SHFY-2022-002). We acknowledge the computation support from the Center for High Performance Computing at Shanghai Jiao Tong University.

Appendix A. Supplementary data

Supplementary data to this article can be found online at https://doi.org/10.1016/j.mtphys.2023.101129.

References

[1] X. Shi, L. Chen, C. Uher, Recent advances in high-performance bulk thermoelectric materials, Int. Mater. Rev. 61 (2016) 379–415, https://doi.org/10.1080/09506608.2016.1183075.
[2] V. Adinolfi, E.H. Sargent, Photovoltage field-effect transistors, Nature 542 (2017) 324–327, https://doi.org/10.1038/nature21050.
[3] A.K. Jena, A. Kulkarni, T. Miyasaka, Halide perovskite photovoltaics: background, status, and future prospects, Chem. Rev. 119 (2019) 3036–3103, https://doi.org/10.1021/acs.chemrev.8b00539.
[4] K. Zhao, A.B. Blichfeld, H. Chen, Q. Song, T. Zhang, C. Zhu, D. Ren, R. Hanus, P. Qiu, B.B. Iversen, F. Xu, G.J. Snyder, X. Shi, L. Chen, Enhanced thermoelectric performance through tuning bonding energy in $Cu_2Se_{1-x}S_x$ liquid-like materials, Chem. Mater. 29 (2017) 6367–6377, https://doi.org/10.1021/acs.chemmater.7b01687.
[5] K. Zhao, P. Qiu, X. Shi, L. Chen, Recent advances in liquid-like thermoelectric materials, Adv. Funct. Mater. 30 (2020): 1903867, https://doi.org/10.1002/adfm.201903867.
[6] D. Yang, A. Benton, J. He, X. Tang, Novel synthesis recipes boosting thermoelectric study of A_2Q (A = Cu, Ag; Q = S, Se, Te), J. Phys. Appl. Phys. 53 (2020): 193001, https://doi.org/10.1088/1361-6463/ab70c5.
[7] T. Wei, P. Qiu, K. Zhao, X. Shi, L. Chen, Ag_2Q-Based (Q = S, Se, Te) silver chalcogenide thermoelectric materials, Adv. Mater. 35 (2023): 2110236, https://doi.org/10.1002/adma.202110236.
[8] D. Yang, X. Su, F. Meng, S. Wang, Y. Yan, J. Yang, J. He, Q. Zhang, C. Uher, M. G. Kanatzidis, X. Tang, Facile room temperature solventless synthesis of high thermoelectric performance Ag_2Se *via* a dissociative adsorption reaction, J. Mater. Chem. A. 5 (2017) 23243–23251, https://doi.org/10.1039/C7TA08726H.
[9] A.K. Gautam, N. Khare, Enhanced thermoelectric figure of merit at near room temperature in n-type binary silver telluride nanoparticles, J. Materiomics. (2022), https://doi.org/10.1016/j.jmat.2022.10.003.
[10] X. Shi, H. Chen, F. Hao, R. Liu, T. Wang, P. Qiu, U. Burkhardt, Y. Grin, L. Chen, Room-temperature ductile inorganic semiconductor, Nat. Mater. 17 (2018) 421–426, https://doi.org/10.1038/s41563-018-0047-z.
[11] Q. Yang, S. Yang, P. Qiu, L. Peng, T.-R. Wei, Z. Zhang, X. Shi, L. Chen, Flexible thermoelectrics based on ductile semiconductors, Science 377 (2022) 854–858, https://doi.org/10.1126/science.abq0682.
[12] J. Liang, T. Wang, P. Qiu, S. Yang, C. Ming, H. Chen, Q. Song, K. Zhao, T.-R. Wei, D. Ren, Y.-Y. Sun, X. Shi, J. He, L. Chen, Flexible thermoelectrics: from silver chalcogenides to full-inorganic devices, Energy Environ. Sci. 12 (2019) 2983–2990, https://doi.org/10.1039/C9EE01777A.
[13] S. Yang, Z. Gao, P. Qiu, J. Liang, T. Wei, T. Deng, J. Xiao, X. Shi, L. Chen, Ductile $Ag_{20}S_7Te_3$ with excellent shape-conformability and high thermoelectric performance, Adv. Mater. (2021): 2007681, https://doi.org/10.1002/adma.202007681.
[14] L. Peng, S. Yang, T.-R. Wei, P. Qiu, J. Yang, Z. Zhang, X. Shi, L. Chen, Phase-modulated mechanical and thermoelectric properties of $Ag_2S_{1-x}Te_x$ ductile semiconductors, J. Materiomics. 8 (2022) 656–661, https://doi.org/10.1016/j.jmat.2021.11.007.
[15] Y. Wang, A. Li, H. Hu, C. Fu, T. Zhu, Reversible room temperature brittle-plastic transition in $Ag_2Te_{0.6}S_{0.4}$ inorganic thermoelectric semiconductor, Adv. Funct. Mater. (2023): 2300189, https://doi.org/10.1002/adfm.202300189.
[16] X. Liang, C. Wang, D. Jin, Influence of nonstoichiometry point defects on electronic thermal conductivity, Appl. Phys. Lett. 117 (2020): 213901, https://doi.org/10.1063/5.0031353.
[17] S. Huang, T.-R. Wei, H. Chen, J. Xiao, M. Zhu, K. Zhao, X. Shi, Thermoelectric Ag_2Se: imperfection, homogeneity, and reproducibility, ACS Appl. Mater. Interfaces 13 (2021) 60192–60199, https://doi.org/10.1021/acsami.1c18483.
[18] T. Wang, K. Zhao, P. Qiu, Q. Song, L. Chen, X. Shi, Aguilarite Ag_4SSe thermoelectric material: natural mineral with low lattice thermal conductivity, ACS Appl. Mater. Interfaces 11 (2019) 12632–12638.
[19] T. Zhu, H. Bai, J. Zhang, G. Tan, Y. Yan, W. Liu, X. Su, J. Wu, Q. Zhang, X. Tang, Realizing high thermoelectric performance in Sb-doped Ag_2Te compounds with a low-temperature monoclinic structure, ACS Appl. Mater. Interfaces 12 (2020) 39425–39433, https://doi.org/10.1021/acsami.0c10932.
[20] O. Alekberov, Z. Jahangirli, R. Paucar, S. Huseynova, N. Abdulzade, A. Nakhmedov, K. Wakita, N. Mamedov, Band structure and vacancy formation in β-Ag_2S: *ab-initio* study: band structure and vacancy formation in β-Ag_2S: *ab-initio* study, Phys. Status Solidi C 12 (2015) 672–675, https://doi.org/10.1002/pssc.201400335.
[21] C. Du, J. Tian, X. Liu, Effect of intrinsic vacancy defects on the electronic properties of monoclinic Ag_2S, Mater. Chem. Phys. 249 (2020): 122961, https://doi.org/10.1016/j.matchemphys.2020.122961.
[22] R. Dalven, R. Gill, Energy gap in β-Ag_2Se, Phys. Rev. 159 (1967) 645–649, https://doi.org/10.1103/PhysRev.159.645.
[23] R. Dalven, R. Gill, Energy gap in β-Ag_2Te, Phys. Rev. 143 (1966) 666–670, https://doi.org/10.1103/PhysRev.143.666.
[24] J. Paier, M. Marsman, K. Hummer, G. Kresse, I.C. Gerber, J.G. Ángyán, Screened hybrid density functionals applied to solids, J. Chem. Phys. 124 (2006): 154709, https://doi.org/10.1063/1.2187006.
[25] R. Ramprasad, H. Zhu, P. Rinke, M. Scheffler, New perspective on formation energies and energy levels of point defects in nonmetals, Phys. Rev. Lett. 108 (2012): 066404, https://doi.org/10.1103/PhysRevLett.108.066404.
[26] M. Shishkin, G. Kresse, Self-consistent *GW* calculations for semiconductors and insulators, Phys. Rev. B 75 (2007): 235102, https://doi.org/10.1103/PhysRevB.75.235102.
[27] C. Freysoldt, B. Grabowski, T. Hickel, J. Neugebauer, G. Kresse, A. Janotti, C. G. Van de Walle, First-principles calculations for point defects in solids, Rev. Mod. Phys. 86 (2014) 253–305, https://doi.org/10.1103/RevModPhys.86.253.
[28] S. Lany, A. Zunger, Assessment of correction methods for the band-gap problem and for finite-size effects in supercell defect calculations: case studies for ZnO and GaAs, Phys. Rev. B 78 (2008): 235104, https://doi.org/10.1103/PhysRevB.78.235104.
[29] H. Peng, D.O. Scanlon, V. Stevanovic, J. Vidal, G.W. Watson, S. Lany, Convergence of density and hybrid functional defect calculations for compound semiconductors, Phys. Rev. B 88 (2013): 115201, https://doi.org/10.1103/PhysRevB.88.115201.
[30] B.R. Ortiz, P. Gorai, V. Stevanović, E.S. Toberer, Thermoelectric performance and defect chemistry in n-type zintl $KGaSb_4$, Chem. Mater. 29 (2017) 4523–4534, https://doi.org/10.1021/acs.chemmater.7b01217.

[31] A. Goyal, P. Gorai, E.S. Toberer, V. Stevanović, First-principles calculation of intrinsic defect chemistry and self-doping in PbTe, Npj Comput, Mater 3 (2017) 42, https://doi.org/10.1038/s41524-017-0047-6.
[32] M.Y. Toriyama, J. Qu, G.J. Snyder, P. Gorai, Defect chemistry and doping of BiCuSeO, J. Mater. Chem. A. 9 (2021) 20685–20694, https://doi.org/10.1039/D1TA05112A.
[33] G. Kresse, J. Furthmüller, Efficiency of ab-initio total energy calculations for metals and semiconductors using a plane-wave basis set, Comput. Mater. Sci. 6 (1996) 15–50, https://doi.org/10.1016/0927-0256(96)00008-0.
[34] P.E. Blöchl, Projector augmented-wave method, Phys. Rev. B 50 (1994) 17953–17979, https://doi.org/10.1103/PhysRevB.50.17953.
[35] J.P. Perdew, K. Burke, M. Ernzerhof, Generalized gradient approximation made simple, Phys. Rev. Lett. 77 (1996) 3865–3868, https://doi.org/10.1103/PhysRevLett.77.3865.
[36] J. Sun, A. Ruzsinszky, J.P. Perdew, Strongly constrained and appropriately normed semilocal density functional, Phys. Rev. Lett. 115 (2015): 036402, https://doi.org/10.1103/PhysRevLett.115.036402.
[37] J. Heyd, G.E. Scuseria, M. Ernzerhof, Hybrid functionals based on a screened Coulomb potential, J. Chem. Phys. 118 (2003) 8207–8215, https://doi.org/10.1063/1.1564060.
[38] S. Grimme, S. Ehrlich, L. Goerigk, Effect of the damping function in dispersion corrected density functional theory, J. Comput. Chem. 32 (2011) 1456–1465, https://doi.org/10.1002/jcc.21759.
[39] H. Peng, Z.-H. Yang, J.P. Perdew, J. Sun, Versatile van der Waals density functional based on a meta-generalized gradient approximation, Phys. Rev. X 6 (2016): 041005, https://doi.org/10.1103/PhysRevX.6.041005.
[40] V.I. Anisimov, O. Gunnarsson, Density-functional calculation of effective Coulomb interactions in metals, Phys. Rev. B 43 (1991) 7570–7574, https://doi.org/10.1103/PhysRevB.43.7570.
[41] M. Cococcioni, S. de Gironcoli, Linear response approach to the calculation of the effective interaction parameters in the LDA + U method, Phys. Rev. B 71 (2005): 035105, https://doi.org/10.1103/PhysRevB.71.035105.
[42] J.A. Suárez, J.J. Plata, A.M. Márquez, J.F. Sanz, Structural, electronic and optical properties of copper, silver and gold sulfide: a DFT study, Theor. Chem. Acc. 135 (2016) 70, https://doi.org/10.1007/s00214-016-1832-x.
[43] J.C. Fuggle, P. Bennett, F.U. Hillebrecht, A. Lenselink, G.A. Sawatzky, Influence of multiplet splittings in high-polarity states on magnetism in transition metals, Phys. Rev. Lett. 49 (1982) 1787–1790, https://doi.org/10.1103/PhysRevLett.49.1787.
[44] C.M. Fang, R.A. de Groot, G.A. Wiegers, Ab initio band structure calculations of the low-temperature phases of Ag_2Se, Ag_2Te and Ag_3AuSe_2, J. Phys. Chem. Solid. 63 (2002) 457–464, https://doi.org/10.1016/S0022-3697(01)00160-3.
[45] S. Kashida, N. Watanabe, T. Hasegawa, H. Iida, M. Mori, S. Savrasov, Electronic structure of Ag_2S, band calculation and photoelectron spectroscopy, Solid State Ionics 158 (2003) 167–175, https://doi.org/10.1016/S0167-2738(02)00768-3.
[46] C. Xiao, J. Xu, K. Li, J. Feng, J. Yang, Y. Xie, Superionic phase transition in silver chalcogenide nanocrystals realizing optimized thermoelectric performance, J. Am. Chem. Soc. 134 (2012) 4287–4293, https://doi.org/10.1021/ja2104476.
[47] R. Sadanaga, S. Sueno, X-ray study on the α-β transition of Ag_2S, Mineral. J. 5 (1967) 124–143.
[48] G. Wiegers, The crystal structure of the low-temperature form of silver selenide, Am. Mineral. J. Earth Planet. Mater. 56 (1971) 1882–1888.
[49] C. Manolikas, A study by means of electron microscopy and electron diffraction of the phase transformation and the domain structure in Ag_2Te, J. Solid State Chem. 66 (1987) 1–6, https://doi.org/10.1016/0022-4596(87)90214-3.
[50] C.G. Van de Walle, J. Neugebauer, First-principles calculations for defects and impurities: applications to III-nitrides, J. Appl. Phys. 95 (2004) 3851–3879, https://doi.org/10.1063/1.1682673.
[51] D. Broberg, B. Medasani, N.E.R. Zimmermann, G. Yu, A. Canning, M. Haranczyk, M. Asta, G. Hautier, PyCDT: a Python toolkit for modeling point defects in semiconductors and insulators, Comput. Phys. Commun. 226 (2018) 165–179, https://doi.org/10.1016/j.cpc.2018.01.004.
[52] C. Freysoldt, J. Neugebauer, C.G. Van de Walle, Fully *ab initio* finite-size corrections for charged-defect supercell calculations, Phys. Rev. Lett. 102 (2009): 016402, https://doi.org/10.1103/PhysRevLett.102.016402.
[53] R. Nelson, C. Ertural, J. George, V.L. Deringer, G. Hautier, R. Dronskowski, LOBSTER: local orbital projections, atomic charges, and chemical-bonding analysis from projector-augmented-wave-based density-functional theory, J. Comput. Chem. 41 (2020) 1931–1940, https://doi.org/10.1002/jcc.26353.
[54] S.P. Ong, W.D. Richards, A. Jain, G. Hautier, M. Kocher, S. Cholia, D. Gunter, V. L. Chevrier, K.A. Persson, G. Ceder, Python Materials Genomics (pymatgen): a robust, open-source python library for materials analysis, Comput. Mater. Sci. 68 (2013) 314–319, https://doi.org/10.1016/j.commatsci.2012.10.028.
[55] V. Wang, N. Xu, J.-C. Liu, G. Tang, W.-T. Geng, VASPKIT: a user-friendly interface facilitating high-throughput computing and analysis using VASP code, Comput. Phys. Commun. 267 (2021): 108033, https://doi.org/10.1016/j.cpc.2021.108033.
[56] W. Mi, P. Qiu, T. Zhang, Y. Lv, X. Shi, L. Chen, Thermoelectric transport of Se-rich Ag_2Se in normal phases and phase transitions, Appl. Phys. Lett. 104 (2014): 133903, https://doi.org/10.1063/1.4870509.
[57] S. Ishiwata, Y. Shiomi, J.S. Lee, M.S. Bahramy, T. Suzuki, M. Uchida, R. Arita, Y. Taguchi, Y. Tokura, Extremely high electron mobility in a phonon-glass semimetal, Nat. Mater. 12 (2013) 512–517, https://doi.org/10.1038/nmat3621.
[58] J. Buckeridge, Equilibrium point defect and charge carrier concentrations in a material determined through calculation of the self-consistent Fermi energy, Comput. Phys. Commun. 244 (2019) 329–342, https://doi.org/10.1016/j.cpc.2019.06.017.
[59] L. Li, C. Peng, J. Chen, Z. Ma, Y. Chen, S. Li, J. Wang, C. Wang, Study the effect of alloying on the phase transition behavior and thermoelectric properties of Ag_2S, J. Alloys Compd. 886 (2021): 161241, https://doi.org/10.1016/j.jallcom.2021.161241.
[60] J. Liang, P. Qiu, Y. Zhu, H. Huang, Z. Gao, Z. Zhang, X. Shi, L. Chen, Crystalline structure-dependent mechanical and thermoelectric performance in $Ag_2Se_{1-x}S_x$ system, Research 2020 (2020): 6591981, https://doi.org/10.34133/2020/6591981.
[61] M. Jin, J. Liang, P. Qiu, H. Huang, Z. Yue, L. Zhou, R. Li, L. Chen, X. Shi, Investigation on low-temperature thermoelectric properties of Ag_2Se polycrystal fabricated by using zone-melting method, J. Phys. Chem. Lett. 12 (2021) 8246–8255, https://doi.org/10.1021/acs.jpclett.1c02139.
[62] M. Ferhat, J. Nagao, Thermoelectric and transport properties of β-Ag_2Se compounds, J. Appl. Phys. 88 (2000) 813–816, https://doi.org/10.1063/1.373741.
[63] H. Wang, W. Chu, D. Wang, W. Mao, W. Pan, Y. Guo, Y. Xiong, H. Jin, Low-temperature thermoelectric properties of β-Ag_2Se synthesized by hydrothermal reaction, J. Electron. Mater. 40 (2011) 624–628, https://doi.org/10.1007/s11664-010-1484-x.